# Evolution of a plasma vortex in air

Cheng-Mu Tsai and Hong-Yu Chu
*Department of Physics, National Chung Cheng University, Chiayi 62102, Taiwan*
(Received 24 August 2015; revised manuscript received 11 November 2015; published 11 January 2016)

We report the generation of a vortex-shaped plasma in air by using a capacitively coupled dielectric barrier discharge system. We show that a vortex-shaped plasma can be produced inside a helium gas vortex and is capable of propagating for 3 cm. The fluctuation of the plasma ring shows a scaling relation with the Reynolds number of the vortex. The transient discharge reveals the property of corona discharge, where the conducting channel within the gas vortex and the blur plasma emission are observed at each half voltage cycle.

DOI: 10.1103/PhysRevE.93.013205

## I. INTRODUCTION

An atmospheric pressure plasma jet has been studied to discover the advantages in biomedical application and surface treatment. It has been operated in various devices and under various conditions, such as kHz, MHz, and microwave power sources [1–4] and different gas concentrations [4–9]. By optimization of the performance of the plasma system, the length of the plasma jet can be a few millimeters to more than 10 cm [8]. It has been reported that the short time observation of the continuous plasma jet was, in fact, a segment of plasma like a plasma bullet in the gas jet [10–13]. The interaction of the plasma bullet and the gas jet was investigated by Jiang *et al.* [7]; they found that the gas flow is able to gain a forward momentum from the discharge.

In previous investigations, researchers have produced toroidal-shaped plasma by using a power source with a large current supply and a magnetic field [14–16]. A high-current discharge between coaxial electrodes was shot out from a plasma gun and passed through a radial magnetic field. The magnetic plasma ring was produced while the magnetic field was stretched and wrapped around the plasma ring. Here, instead of using a large current and a magnetic field to produce ring-shaped plasma, we simply take advantage of the gas vortex being a membraneless ring-structured plasma chamber. The ring-shaped gas vortex can be found in the smoke ring and in the bubble ring generated by a dolphin. It has been extensively studied for years and attracted people's attention not only for its beautiful localized structure but also because of its unstable effect on the interface and the fact that it is one of the prototype examples of interfacial instability problems. The vortex is induced by the velocity shear or the velocity difference between two fluids, which is well-known as the Kelvin-Helmholtz instability [17,18].

In this study, we report an experimental investigation on the generation of a vortex-shaped plasma in open air by using a dielectric barrier discharge setup. We show that the vortex-shaped plasma is able to propagate for 3 cm and for several milliseconds. By using the capacitively coupled dielectric barrier discharge setup, a ring-shaped plasma is produced in a helium gas vortex. We observe that the presence of the plasma greatly affects the propagation of the helium vortex. The fluctuation of the ring-shaped plasma shows a scaling relation with the Reynolds number of the gas vortex. The plasma vortex shows the property of corona discharge in the beginning and transforms to a streamerlike discharge while it propagates away from the powered electrode.

## II. EXPERIMENTAL SETUP

The experiment was conducted in a capacitively coupled dielectric barrier discharge setup as shown in Fig. 1. The helium gas ring was generated by the impact of the pneumatic piston and the motion of the piston was controlled by the pressure of the compressed gas. The gas vortex was observed and recorded by a mirror-type Schlieren system. The nozzle of the chamber with a diameter of 24 mm was surrounded by the high-voltage ring electrode. An aluminum ring with an inner diameter of 22 mm served as a floating ring electrode and was placed inside the nozzle. The inner ring was capacitively coupled and initiated the breakdown of the helium gas in the chamber. An indium tin oxide (ITO) coated glass served as the ground electrode and the dielectric barrier. A mass flow controller (GFC-200, KOFLOC) was used to control the inlet flow of the helium gas into the chamber. The two electrodes were seperated by 4 cm. The discharge was operated by a sinusoid voltage of 10–20 kV (peak-to-peak voltage) and 20 kHz. A high-voltage probe (HVP-28HF, Pintek) and a current probe (2877, Pearson) were used to monitor the voltage and current wave form and recorded by a digital oscilloscope (44Xs, LeCroy). A Spectrometer (USB2000+, Ocean Optics)

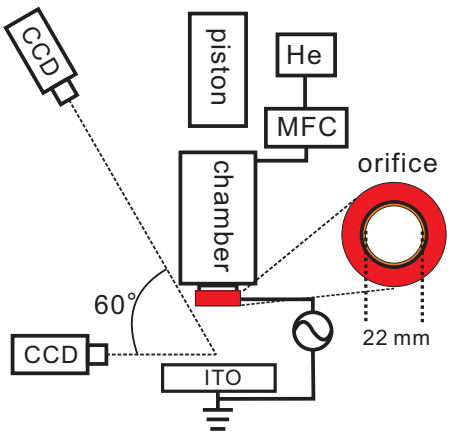


FIG. 1. Schematic diagram of the experimental setup. Inset: An aluminum ring with a diameter of 22 mm is capacitively coupled as a floating ring electrode.

 

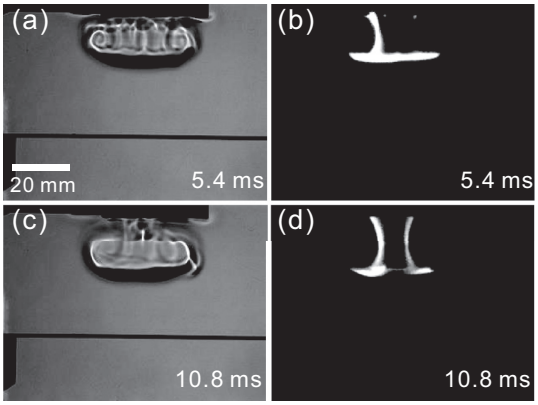


FIG. 2. Panesl (a) and (c) are the helium gas vortex observed by the Schlieren system. Panels (b) and (d) are the corresponding direct observations of the plasma vortex.

was employed to record the plasma emission spectrum and to monitor the density ratio of the helium gas and air. The plasma vortex was recorded by a digital camera (F-032B, AVT Corporation) and an intensified charged-coupled device (ICCD) (DH712, Andor Technology).

### III. RESULTS AND DISCUSSION

The experiment was conducted by first filling the chamber with helium gas and then applying high voltage to initiate the gas breakdown in the chamber. We monitored the emission intensity at 706 nm from helium and 370 nm from nitrogen. While generating the plasma vortex, the intensity ratio of $I_{706}/I_{370}$ was fixed at 2.0 to avoid the effect of different gas concentrations. After the sudden impact from the piston, a gas vortex was generated and observed from the nozzle of the chamber. The supply of the helium gas was shut off in order to not perturb the gas flow in the chamber before generating the vortex. Figures 2(a) and 2(c) show the downward traveling gas vortex and Figs. 2(b) and 2(d) show the corresponding plasma emission. The time for generating the vortex was set as time zero, and the corresponding time is labeled in the corner of each image. Both the gas vortex and the plasma vortex are recorded by two cameras at 370 fps with an exposure of 1 ms. Figure 2 reveals that the plasma ring appears at the lower part of the gas vortex and it travels downward with the gas vortex. Without turning on the plasma, a smooth vortex ring is visualized via the Schlieren observation method.

Figure 3 shows the sequential images of the plasma ring observed from an oblique angle. A circular plasma ring is observed and at a later stage in Fig. 3(d) some plasma filaments are observed on the outer rim of the plasma ring. The filaments

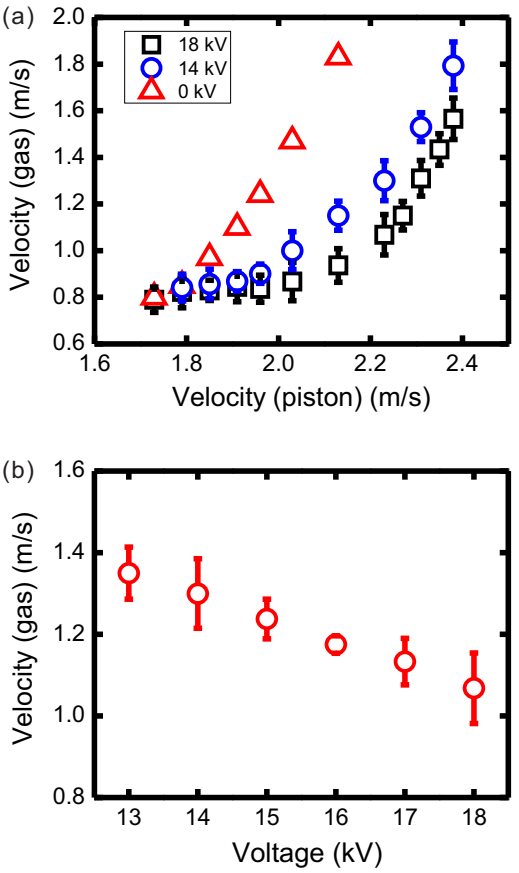


FIG. 4. The traveling speed of the gas vortex at different applied voltages. (a) The traveling speed of the gas vortex without applying voltage is labeled with red triangles. It travels faster with faster impulse of the piston. The gas vortex travels slower while the plasma is generated inside the vortex. The speeds of the gas vortex when applying 14 and 18 kV are labeled with blue circles and black squares, respectively. (b) The traveling speed of the vortex is slower with higher applied voltages. The velocity of the piston is fixed at 2.23 m/s.

on the rim are hard to identify from the observation in Fig. 2. It is noticed that the core of the plasma ring is always connected by the discharge from the power electrode. Here, the plasma vortex shows that it is capable of traveling for a distance of 3 cm and of keeping the form of the vortex for a lifetime of about 10.8 ms.

The propagation of the plasma vortex is associated with the gas vortex. However, the presence of the plasma vortex strongly affects the traveling of the gas vortex. Figure 4(a) shows the traveling speed of the gas vortex at different applied

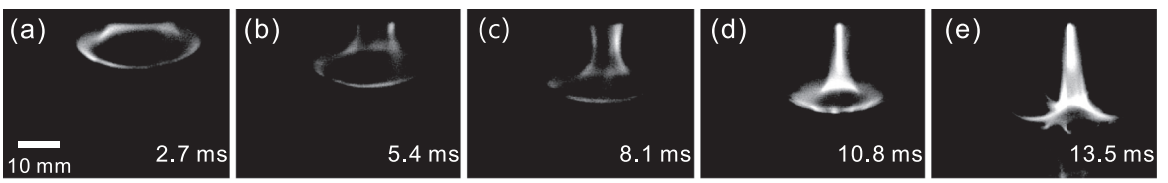


FIG. 3. Observation from a tilting angle shows that the propagation of the plasma vortex is associated with the gas vortex. The plasma filaments are observed on the plasma ring at the later stage. The streamerlike discharge is observed while it travels near the ground electrode.

voltages. The propagation of the vortex is controlled by the impact speed of the pneumatic piston. Surprisingly, it is seen that the traveling speed of the gas vortex can be manipulated by the applied voltages. Without applying the voltage, the faster gas vortex is generated by the higher impact speed of the piston. However, the trend of the vortex speed still remains the same while applying the high voltage, but the gas vortex seems to be dragged by the presence of the plasma. Figure 4(b) shows that the gas vortex travels slower at higher voltages. It is suspected that the discharge in the gas vortex is a heating source to the helium gas and air which slightly increases the temperature of the gas vortex and consequently decreases the density of the gas. The presence of the plasma also perturbs the streaming flow in the helium gas vortex, which affects the circulation of the gas vortex. In fact the discharge repeatedly perturbs the flow in the vortex at a frequency of 20 kHz as shown in Fig. 6. This might contribute to the drag on the gas vortex.

While producing the gas vortex at a higher speed, a wavy vortex is observed which has been reported in Refs. [18–21]. The wavy gas vortex is visualized by the Schlieren system and is shown in Fig. 5(a). The gas chamber was slightly tilted for better observation. The propagating direction of the vortex is not along the gravity direction while conducting the experiment in Fig. 5(a). Figures 5(b)–5(f) show the evolution of the wavy plasma vortex. It is observed that the circular plasma ring fluctuates [mode = 5 in Fig. 5(d)] and the fluctuating plasma ring becomes plasma filaments at the later stages. The discharge that connects the plasma ring and the power electrode seems brighter while the plasma vortex approaches the grounded electrode. The number of filamentary fingers at the later stage seems preselected while the plasma ring is a wavy plasma vortex at the initial stage. The helium gas ring still maintains the shape of the wavy vortex until it reaches to the grounded electrode. It is noticed that the filament number of a wavy plasma vortex is less than that of a smooth plasma vortex as shown in Fig. 3(e).

The mode number $n$ of a wavy vortex was reported following the scaling relation with the Reynolds number Re, i.e., $n \propto \mathrm{Re}^m$. The Reynolds number is $\mathrm{Re} = vl/\nu$, where $\nu$ is the kinematic viscosity of air, and $v$ and $l$ are the speed and the characteristic length of the vortex, respectively. The exponent $m$ is expected in the range of 1/2–1/4 [21]. However, it can be seen that there is a transition of the fluctuation of the plasma ring. Figure 5(g) shows the mode number of the plasma ring as a function of the Reynolds number. It is different from the ordinary model for the air vortex ring $n \propto \mathrm{Re}^m$. We therefore used $n \propto (\mathrm{Re} - \mathrm{Re}_c)^m$ to describe the change of the mode number and the critical onset of the fluctuation at the Reynolds number $\mathrm{Re}_c$. It is found that the fluctuation of the plasma ring appears when the Reynolds number is larger than 2200 and $m = 1/3.18$. Here we are unable to explain why there is an onset of fluctuation of the plasma ring and are unable to conduct experiments in the higher Reynolds number region to verify the scaling relation.

We further conducted experiments to observe the breakdown process using an ICCD. Because the discharge current profile was too weak to be detected, a photomultiplier tube (PMT) was employed to record the discharge emission intensity, which shows different emission intensities at each

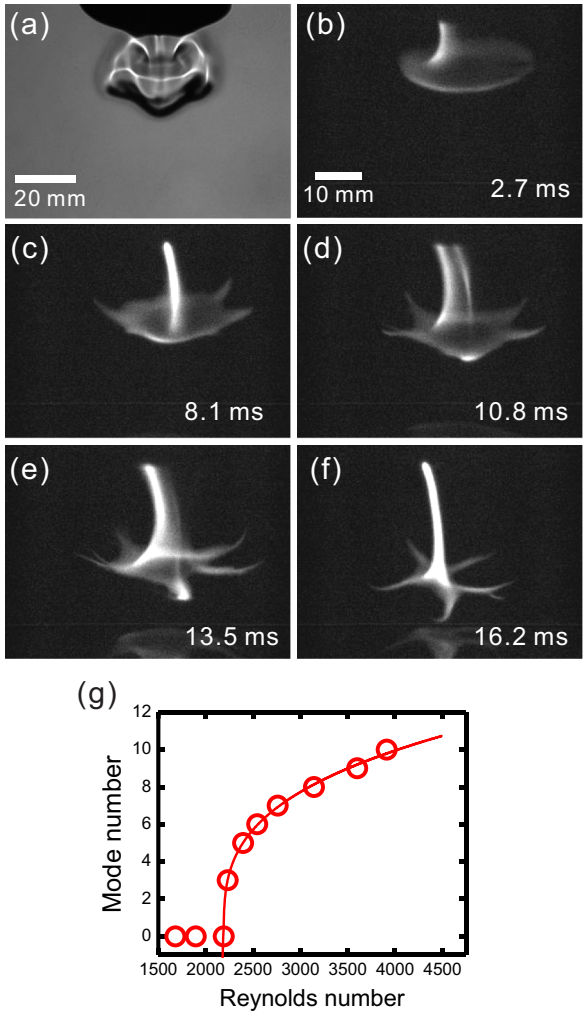


FIG. 5. The wavy gas vortex and the plasma vortex. (a) The fluctuation of the gas vortex is observed and the vortex keeps the wavy shape until it reaches the ground electrode. (b)–(f) The fluctuation of the ring-shaped plasma is observed. The wavy plasma ring transforms into some plasma filaments at the later stage. The number of plasma filaments are found consistent with the mode number of the fluctuating plasma ring. (g) The wavy plasma ring is observed when the Reynolds number of the gas vortex is larger than 2200. The number of fluctuations of the plasma ring increases with the Reynolds number of the gas vortex.

half voltage cycle in Fig 6(e). Figures 6(a)–6(c) show the plasma vortex at different discharge stages while the electrode is positively biased. The insets show the emission intensities from the PMT measurements and the corresponding exposures of the ICCD are shown by the gray regions. A thin plasma filament is observed in Fig. 6(a). It reveals that the breakdown initiates from the power electrode and through the helium gas. Then the discharge propagates and diffuses in the ring structure as shown in Figs. 6(b) and 6(c). In the last stage of the breakdown, the discharge fades out. Figure 6(d) shows the plasma vortex in the positive half cycle at an exposure of 25 $\mu$s. Figures 6(f)–6(h) show the plasma vortex in the negative half cycle. The ring-shaped plasma is no longer observed when the electrode is negatively biased. It is only observed that some

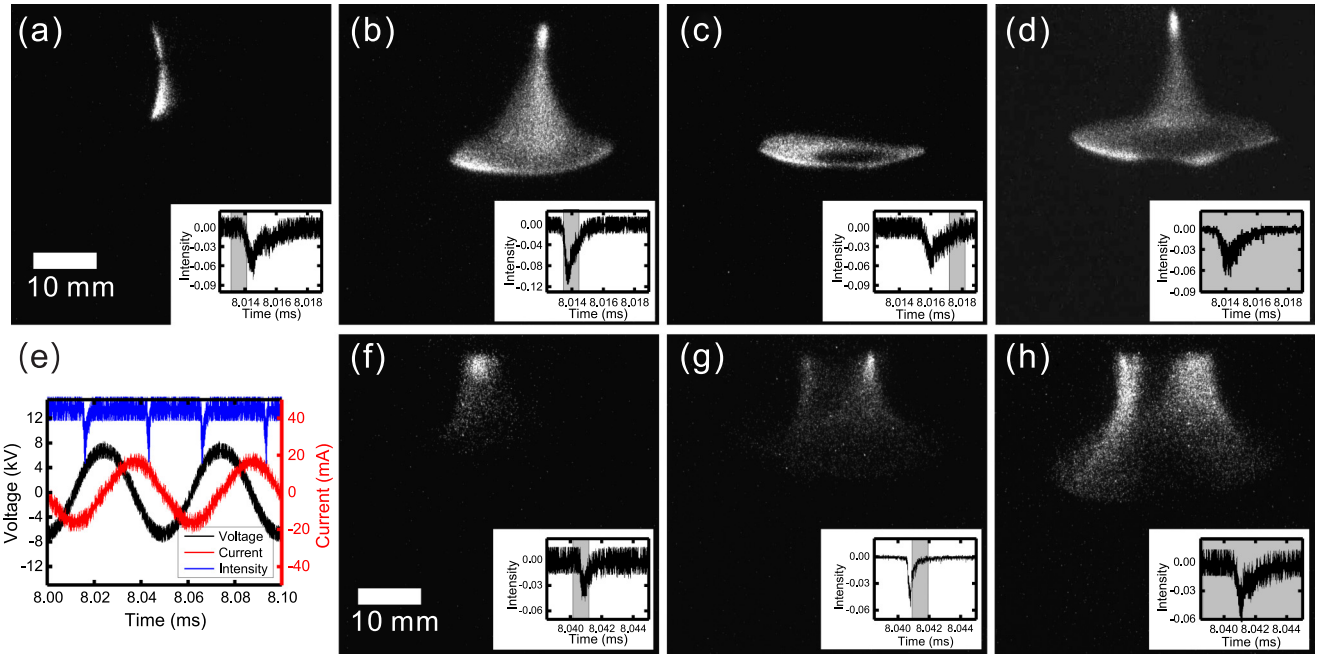


FIG. 6. ICCD observations on the plasma vortex at different half voltage cycle. (a)–(c) The plasma vortex at different stages of the breakdown process while the electrode is positively biased. Insets show the exposure of the ICCD (in the gray region) with respect to the PMT signal. The discharge is found propagating and diffusing in the gas ring. (d) The emission of the plasma vortex within one discharge event in a positive half cycle. (e) The voltage, current, and PMT signal of the plasma vortex experiment. The light emission from the PMT signal shows the breakdown process occurs twice in a voltage cycle. (f) and (g) The plasma vortex at different stages of the breakdown process while the electrode is negatively biased. The discharge is observed as blur emission near the electrode. (h) The emission of the plasma vortex within one discharge event in a negative half cycle.

blur plasma emissions appear near the electrode. Figure 6 indicates that the discharge is a rapid transient process, not a steady one, which is quite different at each half cycle. In the beginning the plasma vortex shows the properties of the corona discharge for the extreme low current and the asymmetric discharge region at each half voltage cycle. The plasma vortex shown in the long time exposure (1 ms) is the combination of the negative corona and the positive corona. After the plasma vortex propagates for about 3 cm, the ring-shaped plasma disappears and transforms into a thin conducting channel. The increasing of the product of the pressure $p$ and distance $d$ (value of $pd$) suggests that the plasma transforms into a streamerlike discharge.

## IV. CONCLUSION

In summary, we have reported the generation of a plasma vortex by using a capacitively coupled dielectric barrier discharge system. The ring-shaped plasma is produced in a helium gas vortex and is capable of propagating for 3 cm. The presence of the plasma in the gas vortex is found to retard the propagation of the gas vortex. The ring-shaped plasma changes from a smooth shape to a wavy shape when the Reynolds number of the gas vortex is larger than 2200. The transient discharge shows a conducting region within the helium gas vortex and a blur plasma emission at each half cycle. This report shows that a plasma vortex can be produced by using a gas vortex as a membraneless ring-structured plasma chamber. It inspires us to produce a plasma tornado or some localized-shaped plasma by carefully designing the gas flow and the electrode apparatus in the future experiments.

## ACKNOWLEDGMENTS

This work was supported by the Ministry of Science and Technology, Taiwan, under Contract No. MOST 102-2112-M-194-008-MY3.

[1] D. B. Kim, J. K. Rhee, B. Gweon, S. Y. Moon, and W. Choe, Appl. Phys. Lett. **91**, 151502 (2007).
[2] J. H. Liu, X. Y. Liu, K. Hu, D. W. Liu, X. P. Lu, F. Iza, and M. G. Kong, Appl. Phys. Lett. **98**, 151502 (2011).
[3] G. Arnoult, R. P. Cardoso, T. Belmonte, and G. Henrion, Appl. Phys. Lett. **93**, 191507 (2008).
[4] D. J. Jin, H. S. Uhm, and G. Cho, Phys. Plasmas **20**, 083513 (2013).
[5] L. Liu, Y. Zhang, W. Tian, Y. Meng, and J. Ouyang, Appl. Phys. Lett. **104**, 244108 (2014).
[6] X. Li, Y. Chang, P. Jia, L. Xu, T. Fang, and L. Wang, Phys. Plasmas **19**, 093504 (2012).

[7] N. Jiang, J. Yang, F. He, and Z. Cao, J. Appl. Phys. **109**, 093305 (2011).
[8] X. Lu, Z. Jiang, Q. Xiong, Z. Tang, X. Hu, and Y. Pan, Appl. Phys. Lett. **92**, 081502 (2008).
[9] T. Shao, C. Zhang, Z. Niu, P. Yan, V. F. Tarasenko, E. Kh. Baksht, A. G. Burahenko, and Y. V. Shut'ko, Appl. Phys. Lett. **98**, 021503 (2011).
[10] M. Teschke, J. Kedzierski, E. G. Finantu-Dinu, D. Korzec, and J. Engemann, IEEE Trans. Plasma Sci. **33**, 310 (2005).
[11] B. Sands, B. Ganguly, and K. Tachibana, Appl. Phys. Lett. **92**, 151503 (2008).
[12] Y. Xian, X. Lu, S. Wu, P. K. Chu, and Y. Pan, Appl. Phys. Lett. **100**, 123702 (2012).
[13] S. Wu, Z. Wang, Q. Huang, X. Tan, X. Lu, and K. Ostrikov, Phys. Plasmas **20**, 023503 (2013).
[14] W. H. Bostick, Phys. Rev. **104**, 292 (1956).
[15] H. Alfven, L. Lindberg, and P. Mitlid, J. Nucl. Energy, Part C **1**, 116 (1960).
[16] L. Lindberg and C. Jacobsen, Astrophys. J. **133**, 1043 (1961).
[17] Lord Kelvin, Philos. Mag. **42**, 362 (1871).
[18] Yu. P. Raizer, *Gas Discharge Physics* (Springer-Verlag, Berlin, 1991).
[19] S. E. Widnall and J. P. Sullivan, Proc. R. Soc. London, Ser. A **332**, 335 (1973).
[20] S. E. Widnall, D. B. Bliss, and C.-Y. Tsai, J. Fluid Mech. **66**, 35 (2006).
[21] T. Maxworthy, J. Fluid Mech. **81**, 465 (2006).